A Correlation Model for Vector Sensor Arrays in Underwater Communication Systems

A. Abdi and H. Guo
Center for Wireless Communication and Signal Processing Research
Dept. of Electrical and Computer Engineering, New Jersey Institute of Technology
Newark, NJ 07102, USA
Emails: abdi@adm.njit.edu, hg45@njit.edu

***Abstract*- A vector sensor measures the scalar and vector components of the acoustic field. Depending on the angle of arrivals and other channel characteristics, different types of correlation appear in a vector sensor array. These correlations affect the performance of a vector sensor communication system. In this paper a new statistical-geometrical framework is developed that provides parametric correlation formulas. These signal correlation expressions are useful for the design and performance analysis of vector sensor communication systems and signal processing algorithms. They can also be useful for estimating some important parameters of the channel such as angle spreads and angle of arrivals. Comparison of the proposed correlation model with experimental data illustrates the usefulness of the model.**

I. INTRODUCTION

A vector sensor can measure non-scalar components of the acoustic field such as the particle velocity, which cannot be obtained by a single scalar (pressure) sensor. In the past, research has been conducted on the application of vector sensors for SONAR and underwater target localization [1]-[7]. Vector sensors and particle velocity channels have recently been proposed and utilized for underwater acoustic communication [8]-[10].

In multipath channels such as shallow waters, a vector sensor receives the signal through several paths. This introduces different levels of correlations in an array of vector sensors. At the system design stage, models for the correlations between pressure and particle velocity channels are highly needed. A system designed without considering the correlations may not provide the anticipated performance [11]-[13]. Closed-form formulas that express pressure-velocity correlations in terms of the channel parameters allow engineers to optimize the system performance. They also help to estimate angle spreads and mean angle of arrivals [14] [15].

II. BASIC DEFINITIONS OF PARTICLE VELOCITY CHANNELS

Consider a vector sensor system implemented in a shallow water channel, as shown in Fig. 1. In the two-dimensional y-z (range-depth) plane, there is one pressure transmitter at the far filed, called Tx and shown by a black dot. We also have two receive vector sensors, represented by two black squares, at $y=0$ and the depths $z=z_1$ and z_1+L, with L as the element spacing. The two receive sensors are called Rx_1 and Rx_2, respectively. The array is located at the depth $z=D$, measured with respect to the center of the array. Each vector sensor measures the pressure, as well as the y and z components of the particle velocity, all in a single co-located point. This means that there are two pressure channels p_1 and p_2, as well as four pressure-equivalent velocity channels p_1^y, p_1^z, p_2^y and p_2^z, all measured in Pascal (Newton/m^2). In Fig. 1 the pressure channels are represented by straight dashed lines, whereas the pressure-equivalent velocity channels are shown by curved dashed lines. To define p_1^y, p_1^z, p_2^y and p_2^z, we need to define the velocity channels v_1^y, v_1^z, v_2^y and v_2^z, in m/s. According to the linearized momentum equation [16], the y and z components of the velocity at locations z_1 and z_1+L of the receive side and at the frequency f_0 can be written as

$$v_1^y=-\frac{1}{j\rho_0\omega_0}\frac{\partial p_1}{\partial y},\quad v_1^z=-\frac{1}{j\rho_0\omega_0}\frac{\partial p_1}{\partial z},$$
$$v_2^y=-\frac{1}{j\rho_0\omega_0}\frac{\partial p_2}{\partial y},\quad v_2^z=-\frac{1}{j\rho_0\omega_0}\frac{\partial p_2}{\partial z}. \tag{1}$$

In the above equations, also known as the Euler's equation, ρ_0 is the density of the fluid in kg/m^3, $j^2=-1$, and $\omega_0=2\pi f_0$ is the frequency in rad/s. Eq. (1) simply states that the velocity in a certain direction is proportional to the spatial pressure gradient in that direction [16] [17]. To simplify the notation, similar to [16], we multiply the velocity channels in (1) with $-\rho_0 c$, the negative of the acoustic impedance of the fluid, where c is the speed of sound in m/s. This gives the associated pressure-equivalent velocity channels as $p_1^y=-\rho_0 c v_1^y$, $p_1^z=-\rho_0 c v_1^z$, $p_2^y=-\rho_0 c v_2^y$, and $p_2^z=-\rho_0 c v_2^z$. With λ as the wavelength in m and $k=2\pi/\lambda=\omega_0/c$ as the wavenumber in rad/m, we finally obtain

$$p_1^y=\frac{1}{jk}\frac{\partial p_1}{\partial y},\quad p_1^z=\frac{1}{jk}\frac{\partial p_1}{\partial z},\quad p_2^y=\frac{1}{jk}\frac{\partial p_2}{\partial y},\quad p_2^z=\frac{1}{jk}\frac{\partial p_2}{\partial z}. \tag{2}$$

Each vector sensor in Fig. 1 provides three output signals. For example, Rx_1 generates one pressure signal r_1 and two pressure-equivalent velocity signals r_1^y and r_1^z, measured in the y and z directions, respectively. If s represent the transmitted signal, then the received signals can be written as

$$r_1=p_1\oplus s+n_1,\qquad r_2=p_2\oplus s+n_2,$$
$$r_1^y=p_1^y\oplus s+n_1^y,\qquad r_2^y=p_2^y\oplus s+n_2^y, \tag{3}$$
$$r_1^z=p_1^z\oplus s+n_1^z,\qquad r_2^z=p_2^z\oplus s+n_2^z.$$

In the above equation $\oplus$ is convolution and each n stands for noise in a particular channel of a specific vector sensor. In the rest of the paper we concentrate on the characterization and analysis of the six channels p_1, p_2, p_1^y, p_1^z, p_2^y and p_2^z.

III. Pressure and Velocity Channel Models

An important multipath underwater channel is the shallow water acoustic channel. It is basically a waveguide, bounded from bottom and the top. The sea floor is a rough surface which introduces scattering, reflection loss, and attenuation by sediments, whereas the sea surface is a rough surface that generates scattering and reflection loss and attenuation by turbidity and bubbles [18]. When compared with deep waters, shallow waters are more complex, due to the many interactions of acoustic waves with boundaries, which result in a significant amount of multipath propagation.

In this paper we develop a statistical/geometrical framework, which concentrates on channel characterization using probabilistic models for the random components of the propagation environment. In this way, the statistical behavior of the channel can be imitated, and convenient closed-form expressions for the correlation functions of interest can be derived. These vector sensor parametric correlation expressions allow engineers to design, simulate, and asses a variety of design schemes under different channel conditions.

In what follows we provide proper statistical representations for pressure and velocity channels in shallow waters. These channel representations will be used later, to calculate different types of channel correlations.

A. Pressure-Related Channel Functions

In this subsection we define and focus on the three pressure channel functions $\chi(\gamma,\tau)$, $p(\tau)$ and $P(f)$, over the angle-delay, delay-space and frequency-space domains, respectively.

Fig. 2 shows the system of Fig. 1, as well as the geometrical details of the received rays in a shallow water channel, with two vector sensor receivers. Two-dimensional propagation of plane waves in the *y*-*z* (range-depth) plane is assumed, in a time-invariant environment with D_0 as the water depth. All the angles are measured with respect to the positive direction of *y*, counterclockwise. We model the rough sea bottom and its surface as collections of N^b and N^s scatterers, respectively, such that $N^b \gg 1$ and $N^s \gg 1$. In Fig. 2, the *i*-th bottom scatterer is represented by S_i^b, $i = 1,2,...,N^b$, whereas S_m^s denotes the *m*-th surface scatterer, $m = 1,2,...,N^s$. Rays scattered from the bottom and the surface are shown by solid thick and solid thin lines, respectively. The rays scattered from S_i^b hit Rx_1 and Rx_2 at the angle-of-arrivals (AOAs) $\gamma_{i,1}^b$ and $\gamma_{i,2}^b$, respectively. The traveled distances are labeled by $\xi_{i,1}^b$ and $\xi_{i,2}^b$, respectively. Similarly, the scattered rays from S_m^s impinge Rx_1 and Rx_2 at the AOAs $\gamma_{m,1}^s$ and $\gamma_{m,2}^s$, respectively, with $\xi_{m,1}^s$ and $\xi_{m,2}^s$ as the traveled distances shown in Fig. 2.

Let τ and γ represent the delay (travel time) and the AOA (measured with respect to the positive direction of *y*, counterclockwise). Then in the angle-delay domain, the impulse responses of the pressure subchannels $Tx-Rx_1$ and $Tx-Rx_2$, represented by $\chi_1(\gamma,\tau)$ and $\chi_2(\gamma,\tau)$, respectively, can be written as

$$\begin{aligned}\chi_1(\gamma,\tau) &= (\Lambda_b/N^b)^{1/2}\sum_{i=1}^{N^b} a_i^b \exp(j\psi_i^b)\delta(\gamma-\gamma_{i,1}^b)\delta(\tau-\tau_{i,1}^b)\\ &+((1-\Lambda_b)/N^s)^{1/2}\sum_{m=1}^{N^s} a_m^s \exp(j\psi_m^s)\delta(\gamma-\gamma_{m,1}^s)\delta(\tau-\tau_{m,1}^s),\end{aligned} \tag{4}$$

$$\begin{aligned}\chi_2(\gamma,\tau) &= (\Lambda_b/N^b)^{1/2}\sum_{i=1}^{N^b} a_i^b \exp(j\psi_i^b)\delta(\gamma-\gamma_{i,2}^b)\delta(\tau-\tau_{i,2}^b)\\ &+((1-\Lambda_b)/N^s)^{1/2}\sum_{m=1}^{N^s} a_m^s \exp(j\psi_m^s)\delta(\gamma-\gamma_{m,2}^s)\delta(\tau-\tau_{m,2}^s).\end{aligned} \tag{5}$$

In eq. (4) and (5), $\delta(.)$ is the Dirac delta, $a_i^b > 0$ and $a_m^s > 0$ represent the amplitudes of the rays scattered from S_i^b and S_m^s, respectively, whereas $\psi_i^b \in [0,2\pi)$ and $\psi_m^s \in [0,2\pi)$ stand for the associated phases. The four delay symbols in (4) and (5) represent the travel times from the bottom and surface scatterers to the two vector sensors. For example, $\tau_{i,1}^b$ denotes the travel time from S_i^b to Rx_1, and so on. As becomes clear in Appendix I, the factors $(N^b)^{-1/2}$ and $(N^s)^{-1/2}$ are included in (4), (5) and the subsequent channel functions, for power normalization. Also $0 \le \Lambda_b \le 1$ represents the amount of the contribution of the bottom scatterers, as explained immediately after eq. (57) in Appendix I. A close to one value for Λ_b indicates that most of the received power is coming from the bottom. Of course the amount of the contribution of the surface is given by $1-\Lambda_b$.

A Dirac delta in the angle domain such as $\delta(\gamma-\tilde{\gamma})$ corresponds to a plane wave with the AOA of $\tilde{\gamma}$, whose equation at an arbitrary point (y,z) is $\exp(jk[y\cos(\tilde{\gamma})+z\sin(\tilde{\gamma})])$. For example, $\delta(\gamma-\gamma_{i,1}^b)$ in (4) represents $\exp(jk\,z_1\sin(\gamma_{i,1}^b))$. This is a plane wave emitted from the scatter S_i^b that impinges Rx_1, located at $y=0$ and $z=z_1$, through the AOA of $\gamma_{i,1}^b$. Using similar plane wave equations for the other angular delta functions in (4) and (5), the impulse responses of the pressure subchannels $Tx-Rx_1$ and $Tx-Rx_2$ in the delay-space domain can be respectively written as

$$\begin{aligned}p_1(\tau) &= (\Lambda_b/N^b)^{1/2}\sum_{i=1}^{N^b} a_i^b \exp(j\psi_i^b)\\ &\times\exp(jk[y\cos(\gamma_{i,1}^b)+z\sin(\gamma_{i,1}^b)])\delta(\tau-\tau_{i,1}^b)\Big|_{y=0,z=z_1}\\ &+((1-\Lambda_b)/N^s)^{1/2}\sum_{m=1}^{N^s} a_m^s \exp(j\psi_m^s)\\ &\times\exp(jk[y\cos(\gamma_{m,1}^s)+z\sin(\gamma_{m,1}^s)])\delta(\tau-\tau_{m,1}^s)\Big|_{y=0,z=z_1},\end{aligned} \tag{6}$$

$$\begin{aligned}p_2(\tau) &= (\Lambda_b/N^b)^{1/2}\sum_{i=1}^{N^b} a_i^b \exp(j\psi_i^b)\\ &\times\exp(jk[y\cos(\gamma_{i,2}^b)+z\sin(\gamma_{i,2}^b)])\delta(\tau-\tau_{i,2}^b)\Big|_{y=0,z=z_1+L}\\ &+((1-\Lambda_b)/N^s)^{1/2}\sum_{m=1}^{N^s} a_m^s \exp(j\psi_m^s)\\ &\times\exp(jk[y\cos(\gamma_{m,2}^s)+z\sin(\gamma_{m,2}^s)])\delta(\tau-\tau_{m,2}^s)\Big|_{y=0,z=z_1+L}.\end{aligned} \tag{7}$$

Based on the definition of the spatial Fourier transform [19], $p_1(\tau)$ and $p_2(\tau)$ can be considered as the spatial Fourier transforms of $\chi_1(\gamma,\tau)$ and $\chi_2(\gamma,\tau)$, respectively, with respect

to γ. The terms y and z in (6) and (7) are intentionally maintained, as in the sequel we need to calculate the spatial gradients of the pressure with respect to y and z, to obtain the velocities.

By taking the Fourier transform of (6) and (7) with respect to τ, we respectively obtain the complex baseband transfer functions of the pressure subchannels $Tx-Rx_1$ and $Tx-Rx_2$ in the frequency-space domain

$$\begin{aligned} P_1(f) &= (\Lambda_b / N^b)^{1/2} \sum_{i=1}^{N^b} a_i^b \exp(j\psi_i^b) \\ &\times \exp(jk[y\cos(\gamma_{i,1}^b) + z\sin(\gamma_{i,1}^b)]) \exp(-j\omega\tau_{i,1}^b)\big|_{y=0,z=z_1} \\ &+ ((1-\Lambda_b)/N^s)^{1/2} \sum_{m=1}^{N^s} a_m^s \exp(j\psi_m^s) \\ &\times \exp(jk[y\cos(\gamma_{m,1}^s) + z\sin(\gamma_{m,1}^s)]) \exp(-j\omega\tau_{m,1}^s)\big|_{y=0,z=z_1}, \end{aligned} \tag{8}$$

$$\begin{aligned} P_2(f) &= (\Lambda_b / N^b)^{1/2} \sum_{i=1}^{N^b} a_i^b \exp(j\psi_i^b) \\ &\times \exp(jk[y\cos(\gamma_{i,2}^b) + z\sin(\gamma_{i,2}^b)]) \exp(-j\omega\tau_{i,2}^b)\big|_{y=0,z=z_1+L} \\ &+ ((1-\Lambda_b)/N^s)^{1/2} \sum_{m=1}^{N^s} a_m^s \exp(j\psi_m^s) \\ &\times \exp(jk[y\cos(\gamma_{m,2}^s) + z\sin(\gamma_{m,2}^s)]) \exp(-j\omega\tau_{m,2}^s)\big|_{y=0,z=z_1+L}, \end{aligned} \tag{9}$$

where $\omega = 2\pi f$ is used to simplify the notation.

B. Velocity-Related Channel Functions

Following the definition of the pressure-equivalent velocity in (2), the velocity channels of interest in the delay-space and frequency-space domains can be written as

$$p_l^y(\tau) = (jk)^{-1}\dot{p}_l(\tau), \quad p_l^z(\tau) = (jk)^{-1}p_l'(\tau), \quad l=1,2, \tag{10}$$

$$P_l^y(f) = (jk)^{-1}\dot{P}_l(f), \quad P_l^z(f) = (jk)^{-1}P_l'(f), \quad l=1,2, \tag{11}$$

where $p_l(\tau)$ and $P_l(f)$, $l=1,2$, are given in (6)-(9). Furthermore, dot and prime denote the partial spatial derivatives $\partial/\partial y$ and $\partial/\partial z$, respectively, of the spatial complex plane waves in (6)-(9). Clearly for $l=1,2$, $p_l^y(\tau)$ and $p_l^z(\tau)$ are the pressure-equivalent impulse responses of the velocity subchannels in the y and z directions, respectively. Moreover, $P_l^y(f)$ and $P_l^z(f)$ represent the pressure-equivalent transfer functions of the velocity subchannels in the y and z directions, respectively, with $l=1,2$.

IV. Correlation Functions in Vector Sensors

In a given shallow water channel, obviously the numerical values of all the amplitudes, phases, AOAs and delays in (6)-(9) are complicated functions of environmental characteristics such as the irregular shape of the sea bottom and its layers/losses, volume microstructures, etc. Due to the uncertainty and complexity in exact determination of all these variables, we model them as random variables. More specifically, we assume all the amplitudes $\{a_i^b\}_i$ and $\{a_m^s\}_m$ are positive uncorrelated random variables, uncorrelated with the phases $\{\psi_i^b\}_i$ and $\{\psi_m^s\}_m$. In addition, all the phases $\{\psi_i^b\}_i$ and $\{\psi_m^s\}_m$ are uncorrelated, uniformly distributed over $[0,2\pi)$. The statistical properties of the AOAs and delays will be discussed later. Overall, all the pressure and velocity channel functions in (6)-(11) are random processes in space, frequency and delay domains. In what follows, first we derive a closed-form expression for the pressure frequency-space correlation. Then we show how other correlations of interest can be calculated from the pressure frequency-space correlation.

The Pressure Frequency-Space Correlation: We define this correlation as $C_P(\Delta f, L) = E[P_2(f+\Delta f)P_1^*(f)]$, where E and * are mathematical expectation and complex conjugate, respectively. In Appendix I we have derived the following expression

$$\begin{aligned} C_P(\Delta f, L) &= \Lambda_b \int_{\gamma^b=0}^{\pi} w_{\text{bottom}}(\gamma^b) \exp(-jT_b\Delta\omega/\sin(\gamma^b)) \\ &\times \exp(jk[\varepsilon_y\cos(\gamma^b) + L\sin(\gamma^b)])d\gamma^b \\ &+ (1-\Lambda_b)\int_{\gamma^s=\pi}^{2\pi} w_{\text{surface}}(\gamma^s) \exp(jT_s\Delta\omega/\sin(\gamma^s)) \\ &\times \exp(jk[\varepsilon_y\cos(\gamma^s) + L\sin(\gamma^s)])d\gamma^s, \quad \text{as} \quad \varepsilon_y \to 0. \end{aligned} \tag{12}$$

In this equation $\Delta\omega = 2\pi\Delta f$ and $\varepsilon_y > 0$ is a small displacement in the y direction, introduced in Appendix I. Moreover, T_b and T_s are defined immediately after (53) in Appendix I. They denote the vertical travel times from the sea bottom to the array center, and from the sea surface to the array center, respectively. Eq. (12) is a frequency-space correlation model for the pressure field which holds for any AOA PDFs with small angle spreads that may be chosen for $w_{\text{bottom}}(\gamma^b)$ and $w_{\text{surface}}(\gamma^s)$. In what follows first we use (12) to derive expressions for various spatial and frequency correlations, which hold for any AOA PDF with small angle spreads. Then in Section V we use a flexible parametric PDF for the AOA, to obtain easy-to-use and closed-from expressions for correlations of practical interest.

Now we provide the following two formulas derived from [20], needed in the sequel to calculate velocity-related correlations. Let $\beta(y,z)$ denote a random field in the two-dimensional range-depth plane. Also let $C_\beta(\ell) = E[\beta(y,z+\ell)\beta^*(y,z)]$ be the spatial correlation in the z direction. Then the correlation functions of the derivative of $\beta(y,z)$ in the z direction, i.e., $\beta'(y,z) = \partial\beta(y,z)/\partial z$ can be written as

$$E\left[\beta(y,z+\ell)\{\beta'(y,z)\}^*\right] = -\partial C_\beta(\ell)/\partial\ell, \tag{13}$$

$$E\left[\beta'(y,z+\ell)\{\beta'(y,z)\}^*\right] = -\partial^2 C_\beta(\ell)/\partial\ell^2. \tag{14}$$

Similar results hold for the derivative of $\beta(y,z)$ in the y direction, i.e., $\dot{\beta}(y,z) = \partial\beta(y,z)/\partial y$.

A. Spatial Correlations for Two Vector Sensors at the Same Frequency

(a) Pressure Correlation: At a fixed frequency with $\Delta f = 0$, the spatial pressure correlation can be obtained from (12) as

$$C_P(0,L) = \int_{\gamma=0}^{2\pi} w(\gamma)\exp(jk[\varepsilon_y\cos(\gamma) + L\sin(\gamma)])d\gamma, \text{ as } \varepsilon_y \to 0, \tag{15}$$

where the overall AOA PDF $w(\gamma)$ is defined as follows, to include both the bottom and surface AOAs

$$w(\gamma) = \Lambda_b w_{\text{bottom}}(\gamma) + (1-\Lambda_b) w_{\text{surface}}(\gamma) . \quad (16)$$

Of course $w_{\text{bottom}}(\gamma) = 0$ for $\pi < \gamma < 2\pi$ and $w_{\text{surface}}(\gamma) = 0$ for $0 < \gamma < \pi$. We main tain (15) as it is, i.e., without replacing ε_y by zero. This is because as we will see in the sequel, we need to take the derivative of $C_P(0,L)$ with respect to ε_y first, then replace ε_y by zero.

(b) Pressure-Velocity Correlations: First we look at the *z*-component of the velocity. Here we are interested in $E[P_2(f)\{P_1^z(f)\}^*] = (-jk)^{-1} E[P_2(f)\{P_1'(f)\}^*]$, where $P_1^z(f)$ is replaced according to (11). On the other hand, similar to (13), one has $E[P_2(f)\{P_1'(f)\}^*] = -\partial E[P_2(f)P_1^*(f)]/\partial L = -\partial C_P(0,L)/\partial L$. Therefore

$$E[P_2(f)\{P_1^z(f)\}^*] = (jk)^{-1}\partial C_P(0,L)/\partial L = \int_{\gamma=0}^{2\pi} w(\gamma)\sin(\gamma) \times \exp(jk[\varepsilon_y \cos(\gamma) + L\sin(\gamma)])d\gamma, \text{ as } \varepsilon_y \to 0, \quad (17)$$

where the integral in (17) is coming from (15). An interesting observation can be made when $w(\gamma)$ is even-symmetric with respect to the *y* axis (symmetry of the AOAs from the bottom and the surface with respect to the horizontal axis *y*). Then with $L = 0$ in (17) we obtain $E[P_1(f)\{P_1^z(f)\}^*] = 0$, i.e., the co-located pressure and *z*-velocity component are uncorrelated.

Now we focus on the *y*-component of the velocity. The correlation of interest is $E[P_2(f)\{P_1^y(f)\}^*] = (-jk)^{-1} E[P_2(f)\{\dot{P}_1(f)\}^*]$, where $P_1^y(f)$ is replaced according to (11). Note that according to the representations for in (55) and (54), respectively, the location of the second vector sensor can be thought of as $(y,z) = (\varepsilon_y, z_1 + L)$, as $\varepsilon_y \to 0$, whereas the first vector sensor is located at $(y,z) = (0,z_1)$. So, using the analogous of (13) in the *y* direction we obtain $E[P_2(f)\{\dot{P}_1(f)\}^*] = -\partial E[P_2(f)P_1^*(f)]/\partial \varepsilon_y$ as $\varepsilon_y \to 0$ $= -\partial C_P(0,L)/\partial \varepsilon_y$ as $\varepsilon_y \to 0$. Differentiation of (15) with respect to ε_y results in

$$E[P_2(f)\{P_1^y(f)\}^*] = (jk)^{-1}\partial C_P(0,L)/\partial \varepsilon_y \text{ as } \varepsilon_y \to 0, = \int_{\gamma=0}^{2\pi} w(\gamma)\cos(\gamma)\exp(jk[\varepsilon_y \cos(\gamma) + L\sin(\gamma)])d\gamma, \text{as } \varepsilon_y \to 0. \quad (18)$$

If $w(\gamma)$ is even-symmetric around the *z* axis, then with $L = 0$ in (18) we obtain $E[P_1(f)\{P_1^y(f)\}^*] = 0$, i.e., the co-located pressure and *y*-velocity component become uncorrelated.

(c) Velocity Correlations: Here we start with the *z*-component of the velocity. We are going to calculate $E[P_2^z(f)\{P_1^z(f)\}^*] = k^{-2} E[P_2'(f)\{P_1'(f)\}^*]$, where $P_2^z(f)$ and $P_1^z(f)$ are replaced according to (11). On the other hand, similar to (14), one can write $E[P_2'(f)\{P_1'(f)\}^*] = -\partial^2 E[P_2(f)P_1^*(f)]/\partial L^2 = -\partial^2 C_P(0,L)/\partial L^2$. Hence

$$E[P_2^z(f)\{P_1^z(f)\}^*] = -k^{-2}\partial^2 C_P(0,L)/\partial L^2 = \int_{\gamma=0}^{2\pi} w(\gamma)\sin^2(\gamma)\exp(jk[\varepsilon_y \cos(\gamma) + L\sin(\gamma)])d\gamma, \text{ as } \varepsilon_y \to 0, \quad (19)$$

where (15) is used to write the integral in (19).

Let us now concentrate on the *y*-component of the velocity. In this case the correlation is $E[P_2^y(f)\{P_1^y(f)\}^*] = k^{-2} E[\dot{P}_2(f)\{\dot{P}_1(f)\}^*]$, in which $P_2^y(f)$ and $P_1^y(f)$ are replaced using to (11). As mentioned before (18), the second and the first vector sensors are located at $(y,z) = (\varepsilon_y, z_1 + L)$, as $\varepsilon_y \to 0$, and $(y,z) = (0,z_1)$, respectively. Thus, by using the equivalent of (14) in the *y* direction we obtain $E[\dot{P}_2(f)\{\dot{P}_1(f)\}^*] = -\partial^2 E[P_2(f)P_1^*(f)]/\partial \varepsilon_y^2$ as $\varepsilon_y \to 0 =$ $-\partial^2 C_P(0,L)/\partial \varepsilon_y^2$ as $\varepsilon_y \to 0$. Taking the second derivative of (15) with respect to ε_y results in

$$E[P_2^y(f)\{P_1^y(f)\}^*] = -k^{-2}\partial^2 C_P(0,L)/\partial \varepsilon_y^2 \text{ as } \varepsilon_y \to 0, = \int_{\gamma=0}^{2\pi} w(\gamma)\cos^2(\gamma)\exp(jk[\varepsilon_y \cos(\gamma) + L\sin(\gamma)])d\gamma, \text{ as } \varepsilon_y \to 0. \quad (20)$$

The (average) received powers via the pressure-equivalent velocity channels in the *z* and *y* directions are $E[|P_1^z(f)|^2]$ and $E[|P_1^y(f)|^2]$, respectively. Using (19) and (20) with $L = 0$, and since $\sin^2(\gamma) < 1$ and $\cos^2(\gamma) < 1$, one can easily show

$$E[|P_1^z(f)|^2] < 1, \; E[|P_1^y(f)|^2] < 1, \quad E[|P_1^z(f)|^2] + E[|P_1^y(f)|^2] = 1. \quad (21)$$

Therefore, the received powers via the two velocity channels are not equal. However, through both of them together we receive the same total power that a pressure sensor collects, as shown by the last equation in (21). Note that in this paper the power received by a pressure sensor is $E[|P_1(f)|^2] = C_P(0,0) = 1$, obtained from (15).

Finally, the correlation between the *z* and *y* components of the velocity is $E[P_2^z(f)\{P_1^y(f)\}^*] = k^{-2} E[P_2'(f)\{\dot{P}_1(f)\}^*]$, with $P_2^z(f)$ and $P_1^y(f)$ substituted according to (11). A straightforward generalization of (14) results in $E[P_2'(f)\{\dot{P}_1(f)\}^*] = -\partial^2 E[P_2(f)P_1^*(f)]/\partial L \partial \varepsilon_y$ as $\varepsilon_y \to 0 =$ $-\partial^2 C_P(0,L)/\partial L \partial \varepsilon_y$ as $\varepsilon_y \to 0$. By taking the derivatives of (15) with respect to *L* and ε_y we obtain

$$E[P_2^z(f)\{P_1^y(f)\}^*] = -k^{-2}\partial^2 C_P(0,L)/\partial L \partial \varepsilon_y, \text{ as } \varepsilon_y \to 0, = \int_{\gamma=0}^{2\pi} w(\gamma)\sin(\gamma)\cos(\gamma)\exp(jk[\varepsilon_y \cos(\gamma) + L\sin(\gamma)])d\gamma, \varepsilon_y \to 0. \quad (22)$$

With $L = 0$, there are two possibilities for which (22) becomes zero: $w(\gamma)$ is even-symmetric with respect to the *y* axis, or $w(\gamma)$ is even-symmetric around the *z* axis. In both cases the co-located *z* and *y* components of the velocity are uncorrelated.

B. Frequency Correlations for One Vector Sensor

(a) Pressure Correlation: With $L = 0$ in (12) we can obtain

$$C_P(\Delta f, 0) = \Lambda_b \int_{\gamma=0}^{\pi} w_{\text{bottom}}(\gamma)\exp(-jT_b\Delta\omega/\sin(\gamma))d\gamma + (1-\Lambda_b)\int_{\gamma=\pi}^{2\pi} w_{\text{surface}}(\gamma)\exp(jT_s\Delta\omega/\sin(\gamma))d\gamma, \quad (23)$$

where γ^b and γ^s in (12) are replaced with γ, to simplify the notation. As mentioned previously, $w_{\text{bottom}}(\gamma)=0$ for $\pi<\gamma<2\pi$ and $w_{\text{surface}}(\gamma)=0$ for $0<\gamma<\pi$.

Pressure-Velocity and Velocity Correlations: The correlations derived in the previous subsection are all derived assuming that there is no frequency separation between the quantities of interest, i.e., $\Delta f=0$. To study frequency correlation for a single vector sensor, one needs to replace $P_2(f)$ in the equations of the previous subsection with $P_1(f+\Delta f)$, which corresponds to $L=0$. This gives the following equations for the frequency correlations of each vector sensor in Fig. 1.

(b) Pressure-Velocity Correlations: The correlations $E[P_1(f+\Delta f)\{P_1^z(f)\}^*]$ and $E[P_1(f+\Delta f)\{P_1^y(f)\}^*]$ can be expressed in terms of the first-order derivatives of , similar to (17) and (18), respectively

$$E[P_1(f+\Delta f)\{P_1^z(f)\}^*]=(jk)^{-1}\partial C_P(\Delta f,L)/\partial L\,|_{L=0}$$
$$=\Lambda_b\int_{\gamma=0}^{\pi}w_{\text{bottom}}(\gamma)\sin(\gamma)\exp(-jT_b\Delta\omega/\sin(\gamma))d\gamma \quad (24)$$
$$+(1-\Lambda_b)\int_{\gamma=\pi}^{2\pi}w_{\text{surface}}(\gamma)\sin(\gamma)\exp(jT_s\Delta\omega/\sin(\gamma))d\gamma,$$

$$E[P_1(f+\Delta f)\{P_1^y(f)\}^*]=(jk)^{-1}\partial C_P(\Delta f,0)/\partial\varepsilon_y\,|_{\varepsilon_y=0}$$
$$=\Lambda_b\int_{\gamma=0}^{\pi}w_{\text{bottom}}(\gamma)\cos(\gamma)\exp(-jT_b\Delta\omega/\sin(\gamma))d\gamma \quad (25)$$
$$+(1-\Lambda_b)\int_{\gamma=\pi}^{2\pi}w_{\text{surface}}(\gamma)\cos(\gamma)\exp(jT_s\Delta\omega/\sin(\gamma))d\gamma.$$

The integrals in (24) and (25) are obtained using the integral representation of $C_P(\Delta f,L)$ in (12).

(c) Velocity Correlations: The correlations $E[P_1^z(f+\Delta f)\{P_1^z(f)\}^*]$, $E[P_1^y(f+\Delta f)\{P_1^y(f)\}^*]$ and $E[P_1^z(f+\Delta f)\{P_1^y(f)\}^*]$ are the second derivatives of $C_P(\Delta f,L)$, similar to (19), (20) and (22), respectively

$$E[P_1^z(f+\Delta f)\{P_1^z(f)\}^*]=-k^{-2}\partial^2C_P(\Delta f,L)/\partial L^2\,|_{L=0}$$
$$=\Lambda_b\int_{\gamma=0}^{\pi}w_{\text{bottom}}(\gamma)\sin^2(\gamma)\exp(-jT_b\Delta\omega/\sin(\gamma))d\gamma \quad (26)$$
$$+(1-\Lambda_b)\int_{\gamma=\pi}^{2\pi}w_{\text{surface}}(\gamma)\sin^2(\gamma)\exp(jT_s\Delta\omega/\sin(\gamma))d\gamma,$$

$$E[P_1^y(f+\Delta f)\{P_1^y(f)\}^*]=-k^{-2}\partial^2C_P(\Delta f,0)/\partial\varepsilon_y^2\,|_{\varepsilon_y=0}$$
$$=\Lambda_b\int_{\gamma=0}^{\pi}w_{\text{bottom}}(\gamma)\cos^2(\gamma)\exp(-jT_b\Delta\omega/\sin(\gamma))d\gamma \quad (27)$$
$$+(1-\Lambda_b)\int_{\gamma=\pi}^{2\pi}w_{\text{surface}}(\gamma)\cos^2(\gamma)\exp(jT_s\Delta\omega/\sin(\gamma))d\gamma,$$

$$E[P_1^z(f+\Delta f)\{P_1^y(f)\}^*]=-k^{-2}\partial^2C_P(\Delta f,L)/\partial L\partial\varepsilon_y\,|_{L=0,\varepsilon_y=0}$$
$$=\Lambda_b\int_{\gamma=0}^{\pi}w_{\text{bottom}}(\gamma)\sin(\gamma)\cos(\gamma)\exp(-jT_b\Delta\omega/\sin(\gamma))d\gamma \quad (28)$$
$$+(1-\Lambda_b)\int_{\gamma=\pi}^{2\pi}w_{\text{surface}}(\gamma)\sin(\gamma)\cos(\gamma)\exp(jT_s\Delta\omega/\sin(\gamma))d\gamma.$$

The integrals in the above three equations are obtained using (12). With $\Delta f=0$, (26) and (27) confirm the average power relations given in (21).

C. Frequency-Space Correlations for Two Vector Sensors

To investigate the frequency-space correlation between the channels of the two vector sensors of Fig. 1, one needs to replace $P_2(f)$ in equations (17)-(20) and (22) with $P_2(f+\Delta f)$. This provides us with the following equations for the frequency-space correlations between the two vector sensor receivers.

(a) Pressure-Velocity Correlations:

$$E[P_2(f+\Delta f)\{P_1^z(f)\}^*]=(jk)^{-1}\partial C_P(\Delta f,L)/\partial L, \quad (29)$$

$$E[P_2(f+\Delta f)\{P_1^y(f)\}^*]=(jk)^{-1}\partial C_P(\Delta f,L)/\partial\varepsilon_y,\ \varepsilon_y\to 0. \quad (30)$$

(b) Velocity Correlations:

$$E[P_2^z(f+\Delta f)\{P_1^z(f)\}^*]=-k^{-2}\partial^2C_P(\Delta f,L)/\partial L^2, \quad (31)$$

$$E[P_2^y(f+\Delta f)\{P_1^y(f)\}^*]=-k^{-2}\partial^2C_P(\Delta f,L)/\partial\varepsilon_y^2,\varepsilon_y\to 0, \quad (32)$$

$$E[P_2^z(f+\Delta f)\{P_1^y(f)\}^*]=-k^{-2}\partial^2C_P(\Delta f,L)/\partial L\partial\varepsilon_y,\varepsilon_y\to 0. \quad (33)$$

For any given $C_P(\Delta f,L)$, the above correlations can be easily calculated by taking the derivates. In what follows, one model for $C_P(\Delta f,L)$ is provided and different types of correlations are calculated.

V. Vector Sensor Correlations Assuming a Gaussian Angle-of-Arrival Model

Here we consider the case where the two-element vector sensor array in Fig. 2 receives signal through two beams: one from the bottom with mean AOA μ_b and angle spread σ_b, and the other one from the surface with mean AOA μ_s and angle spread σ_s. When the angle spreads are small, one can model the AOAs with the following Gaussian PDFs

$$w_{\text{buttom}}(\gamma^b)=(2\pi\sigma_b^2)^{-\frac{1}{2}}\exp[-(\gamma^b-\mu_b)^2/(2\sigma_b^2)],\gamma^b\in(0,\pi),$$
$$w_{\text{surface}}(\gamma^s)=(2\pi\sigma_s^2)^{-\frac{1}{2}}\exp[-(\gamma^s-\mu_s)^2/(2\sigma_s^2)],\gamma^s\in(\pi,2\pi). \quad (34)$$

For large angle spreads, once can use the von Mises PDF [21] [22]. In Fig. 3 these two PDFs are plotted in both linear and polar coordinates.

The first-order Taylor expansion of γ^b around μ_b gives the following results

$$\cos(\gamma^b)\approx\cos(\mu_b)-\sin(\mu_b)(\gamma^b-\mu_b),$$
$$\sin(\gamma^b)\approx\sin(\mu_b)+\cos(\mu_b)(\gamma^b-\mu_b), \quad (35)$$
$$\frac{1}{\sin(\gamma^b)}\approx\frac{1}{\sin(\mu_b)}-\frac{1}{\sin(\mu_b)}\frac{1}{\tan(\mu_b)}(\gamma^b-\mu_b).$$

where $\tan(.)=\sin(.)/\cos(.)$. Of course similar relations can be obtained for γ^s. The utility of these first-order expansions comes from the considered small angle spreads, which means the AOAs γ^b and γ^s are mainly concentrated around μ_b and μ_s, respectively . By substituting these relations into (12), $C_P(\Delta f,L)$ can be written as in (36). The integrals in (36) resemble the characteristic function of a zero-mean Gaussian variable, which can be written as $\int\exp(j\theta x)(2\pi\sigma^2)^{-1/2}\exp[-x^2/(2\sigma^2)]dx=\exp(-\sigma^2\theta^2/2)$ [20]. This simplifies (36) to the closed form in (37).

$$C_P(\Delta f, L) \approx \Lambda_b \exp\begin{pmatrix} jk\varepsilon_y \cos(\mu_b) + jkL\sin(\mu_b) \\ -j[\sin(\mu_b)]^{-1} T_b \Delta\omega \end{pmatrix} \times$$
$$\int_{\gamma^b=0}^{\pi} w_{\text{bottom}}(\gamma^b) \exp\left[j\begin{pmatrix} -k\varepsilon_y \sin(\mu_b) \\ +kL\cos(\mu_b) \\ +[\sin(\mu_b)\tan(\mu_b)]^{-1} T_b \Delta\omega \end{pmatrix} (\gamma^b - \mu_b) \right] d\gamma^b$$
$$+ (1-\Lambda_b) \exp\begin{pmatrix} jk\varepsilon_y \cos(\mu_s) + jkL\sin(\mu_s) \\ +j[\sin(\mu_s)]^{-1} T_s \Delta\omega \end{pmatrix} \times$$
$$\int_{\gamma^s=\pi}^{2\pi} w_{\text{surface}}(\gamma^s) \exp\left[j\begin{pmatrix} -k\varepsilon_y \sin(\mu_s) \\ +kL\cos(\mu_s) \\ -[\sin(\mu_s)\tan(\mu_s)]^{-1} T_s \Delta\omega \end{pmatrix} (\gamma^s - \mu_s) \right] d\gamma^s,$$
as $\varepsilon_y \to 0.$ (36)

$$C_P(\Delta f, L) = \Lambda_b \exp\left[j\begin{pmatrix} k\varepsilon_y \cos(\mu_b) + kL\sin(\mu_b) \\ -[\sin(\mu_b)]^{-1} T_b \Delta\omega \end{pmatrix} \right]$$
$$\times \exp\left[-0.5\sigma_b^2 \begin{pmatrix} -k\varepsilon_y \sin(\mu_b) + kL\cos(\mu_b) \\ +[\sin(\mu_b)\tan(\mu_b)]^{-1} T_b \Delta\omega \end{pmatrix}^2 \right]$$
$$+ (1-\Lambda_b) \exp\left[j\begin{pmatrix} k\varepsilon_y \cos(\mu_s) + kL\sin(\mu_s) \\ +[\sin(\mu_s)]^{-1} T_s \Delta\omega \end{pmatrix} \right] \quad (37)$$
$$\times \exp\left[-0.5\sigma_s^2 \begin{pmatrix} -k\varepsilon_y \sin(\mu_s) + kL\cos(\mu_s) \\ -[\sin(\mu_s)\tan(\mu_s)]^{-1} T_s \Delta\omega \end{pmatrix}^2 \right],$$
as $\varepsilon_y \to 0.$

According to (37) we have $C_P(0,0) = 1$, consistent with the convention of unit (total average) received pressure power, introduced in Appendix I. By taking the derivatives of (37) with respect to L and ε_y, as listed in (29)-(33), closed-form expressions for a variety of correlations in vector sensor receivers can be obtained. In what follows we focus on spatial correlations for two vector sensors at the same frequency and frequency correlations for a single vector sensor.

A. Spatial Correlations for Two Vector Sensors at the Same Frequency

(a) Pressure Correlation: With $\Delta f = 0$, (37) reduces to

$$C_P(0, L) = \Lambda_b \exp\left[jkL\sin(\mu_b) - 0.5\sigma_b^2 k^2 L^2 \cos^2(\mu_b) \right] + (1-\Lambda_b) \exp\left[jkL\sin(\mu_s) - 0.5\sigma_s^2 k^2 L^2 \cos^2(\mu_s) \right]. \quad (38)$$

The magnitude of (38) is plotted in Fig. 4. To show the accuracy of (38), the exact but more complex equation for the pressure correlation is derived in Appendix II, eq. (67), and is plotted in Fig. 4. The close agreement between the two curves verifies the usefulness of the approximate yet simpler pressure spatial correlation model in (38).

(b) Pressure-Velocity Correlations: By taking the derivative of (38) with respect to L we obtain

$$E[P_2(f)\{P_1^z(f)\}^*] = \Lambda_b[\sin(\mu_b) + j\sigma_b^2 kL\cos^2(\mu_b)] \times \exp\left[jkL\sin(\mu_b) - 0.5\sigma_b^2 k^2 L^2 \cos^2(\mu_b) \right] + (1-\Lambda_b)[\sin(\mu_s) + j\sigma_s^2 kL\cos^2(\mu_s)] \times \exp\left[jkL\sin(\mu_s) - 0.5\sigma_s^2 k^2 L^2 \cos^2(\mu_s) \right]. \quad (39)$$

Moreover, differentiation of (37) with respect to ε_y at $\Delta f = 0$ results in

$$E[P_2(f)\{P_1^y(f)\}^*] = \Lambda_b[\cos(\mu_b) - j\sigma_b^2 kL\sin(\mu_b)\cos(\mu_b)] \times \exp\left[jkL\sin(\mu_b) - 0.5\sigma_b^2 k^2 L^2 \cos^2(\mu_b) \right] + (1-\Lambda_b)[\cos(\mu_s) - j\sigma_s^2 kL\sin(\mu_s)\cos(\mu_s)] \times \exp\left[jkL\sin(\mu_s) - 0.5\sigma_s^2 k^2 L^2 \cos^2(\mu_s) \right] \quad (40)$$

For $L = 0$, i.e., a single vector sensor, co-located pressure/vertical-velocity and co-located pressure/horizontal-velocity correlations are $\Lambda_b \sin(\mu_b) + (1-\Lambda_b)\sin(\mu_s)$ and $\Lambda_b \cos(\mu_b) + (1-\Lambda_b)\cos(\mu_s)$, respectively. As an example, let $\Lambda_b = 0.4$, $\sigma_b = \pi/90$ (2°), $\mu_b = \pi/18$ (10°), $\sigma_s = \pi/120$ (1.5°), and $\mu_s = 348\pi/180$ (348° ≡ −12°). This results in -0.055 and 0.98 for P_1/P_1^z and P_1/P_1^y correlations, respectively. Plots of the magnitudes of (39) and (40) are provided in Fig. 4.

(c) Velocity Correlations: By taking the second derivatives of (37) according to (31)-(33) at $\Delta f = 0$ we get

$$E[P_2^z(f)\{P_1^z(f)\}^*] = \Lambda_b \begin{bmatrix} \sin^2(\mu_b) + \sigma_b^2 \cos^2(\mu_b) \\ -\sigma_b^4 k^2 L^2 \cos^4(\mu_b) \\ +j2\sigma_b^2 kL\sin(\mu_b)\cos^2(\mu_b) \end{bmatrix} \times \exp\left[jkL\sin(\mu_b) - 0.5\sigma_b^2 k^2 L^2 \cos^2(\mu_b) \right] + (1-\Lambda_b) \begin{bmatrix} \sin^2(\mu_s) + \sigma_s^2 \cos^2(\mu_s) \\ -\sigma_s^4 k^2 L^2 \cos^4(\mu_s) \\ +j2\sigma_s^2 kL\sin(\mu_s)\cos^2(\mu_s) \end{bmatrix} \times \exp\left[jkL\sin(\mu_s) - 0.5\sigma_s^2 k^2 L^2 \cos^2(\mu_s) \right], \quad (41)$$

$$E[P_2^y(f)\{P_1^y(f)\}^*] = \Lambda_b \begin{bmatrix} \cos^2(\mu_b) + \sigma_b^2 \sin^2(\mu_b) \\ -\sigma_b^4 k^2 L^2 \sin^2(\mu_b)\cos^2(\mu_b) \\ -j2\sigma_b^2 kL\sin(\mu_b)\cos^2(\mu_b) \end{bmatrix} \times \exp\left[jkL\sin(\mu_b) - 0.5\sigma_b^2 k^2 L^2 \cos^2(\mu_b) \right] + (1-\Lambda_b) \begin{bmatrix} \cos^2(\mu_s) + \sigma_s^2 \sin^2(\mu_s) \\ -\sigma_s^4 k^2 L^2 \sin^2(\mu_s)\cos^2(\mu_s) \\ -j2\sigma_s^2 kL\sin(\mu_s)\cos^2(\mu_s) \end{bmatrix} \times \exp\left[jkL\sin(\mu_s) - 0.5\sigma_s^2 k^2 L^2 \cos^2(\mu_s) \right], \quad (42)$$

$$E[P_2^z(f)\{P_1^y(f)\}^*] = \Lambda_b \begin{bmatrix} (1-\sigma_b^2)\sin(\mu_b)\cos(\mu_b) \\ +\sigma_b^4 k^2 L^2 \sin(\mu_b)\cos^3(\mu_b) \\ -jkL\sigma_b^2 \cos(\mu_b)\{\sin^2(\mu_b) - \cos^2(\mu_b)\} \end{bmatrix} \quad (43)$$

$$\times \exp\left[jkL\sin(\mu_b) - 0.5\sigma_b^2 k^2 L^2 \cos^2(\mu_b)\right]$$
$$+(1-\Lambda_b)\begin{bmatrix}(1-\sigma_s^2)\sin(\mu_s)\cos(\mu_s)\\ +\sigma_s^4 k^2 L^2 \sin(\mu_s)\cos^3(\mu_s)\\ -jkL\sigma_s^2\cos(\mu_s)\{\sin^2(\mu_s)-\cos^2(\mu_s)\}\end{bmatrix} \quad (43)$$
$$\times \exp\left[jkL\sin(\mu_s) - 0.5\sigma_s^2 k^2 L^2 \cos^2(\mu_s)\right].$$

For a single vector sensor, by plugging $L=0$ into the above equations we obtain

$$E[|P_1^z(f)|^2] = \Lambda_b[\sin^2(\mu_b)+\sigma_b^2\cos^2(\mu_b)] + (1-\Lambda_b)[\sin^2(\mu_s)+\sigma_s^2\cos^2(\mu_s)] \approx \Lambda_b\sin^2(\mu_b)+(1-\Lambda_b)\sin^2(\mu_s), \quad (44)$$

$$E[|P_1^y(f)|^2] = \Lambda_b[\cos^2(\mu_b)+\sigma_b^2\sin^2(\mu_b)] + (1-\Lambda_b)[\cos^2(\mu_s)+\sigma_s^2\sin^2(\mu_s)] \approx \Lambda_b\cos^2(\mu_b)+(1-\Lambda_b)\cos^2(\mu_s), \quad (45)$$

$$E[P_1^z(f)\{P_1^y(f)\}^*] = \Lambda_b(1-\sigma_b^2)\sin(\mu_b)\cos(\mu_b) + (1-\Lambda_b)(1-\sigma_s^2)\sin(\mu_s)\cos(\mu_s) \approx (1/2)[\Lambda_b\sin(2\mu_b)+(1-\Lambda_b)\sin(2\mu_s)]. \quad (46)$$

The almost equal sign $\approx$ in (44)-(46) comes from the assumption of $\sigma_b, \sigma_s \ll 1$ in this case study. As a numerical example, let $\Lambda_b = 0.4$, $\sigma_b = \pi/90$ (2°), $\mu_b = \pi/18$ (10°), $\sigma_s = \pi/120$ (1.5°), and $\mu_s = 348\pi/180$ ($348^\circ \equiv -12^\circ$). According to (44) and (45), the average powers of the vertical and horizontal velocity channels are 0.038 and 0.962, respectively. Furthermore, the correlation between the vertical and horizontal channels is -0.0536, calculated using (46). Plots of the magnitudes of (41)-(43) are provided in Fig. 5.

B. Frequency Correlations for One Vector Sensor

(a) Pressure Correlation: With $L=0$ in (37) we obtain

$$C_P(\Delta f, 0) = \Lambda_b \exp\left(-j[\sin(\mu_b)]^{-1}T_b\Delta\omega\right) \times \exp\left[-0.5\sigma_b^2[\sin(\mu_b)\tan(\mu_b)]^{-2}T_b^2(\Delta\omega)^2\right] + (1-\Lambda_b)\exp\left(j[\sin(\mu_s)]^{-1}T_s\Delta\omega\right) \times \exp\left[-0.5\sigma_s^2[\sin(\mu_s)\tan(\mu_s)]^{-2}T_s^2(\Delta\omega)^2\right]. \quad (47)$$

The magnitude of (47) is plotted in Fig. 6. To show the accuracy of (47), the exact but more complex equation for the frequency correlation is derived in Appendix II, eq. (67), and is plotted in Fig. 6. The close agreement between the two curves verifies the usefulness of the approximate yet simpler pressure frequency correlation model in (47).

(b) Pressure-Velocity Correlations: By applying (29) and (30) to (37) with $L=0$ one obtains the following results, respectively

$$E[P_1(f+\Delta f)\{P_1^z(f)\}^*] = \Lambda_b[\sin(\mu_b)+j\sigma_b^2[\tan(\mu_b)]^{-2}T_b\Delta\omega]\times \exp\left[-j[\sin(\mu_b)]^{-1}T_b\Delta\omega - 0.5\sigma_b^2[\sin(\mu_b)\tan(\mu_b)]^{-2}T_b^2(\Delta\omega)^2\right] + (1-\Lambda_b)[\sin(\mu_s)-j\sigma_s^2[\tan(\mu_s)]^{-2}T_s\Delta\omega]\times \exp\left[j[\sin(\mu_s)]^{-1}T_s\Delta\omega - 0.5\sigma_s^2[\sin(\mu_s)\tan(\mu_s)]^{-2}T_s^2(\Delta\omega)^2\right], \quad (48)$$

$$E[P_1(f+\Delta f)\{P_1^y(f)\}^*] = \Lambda_b[\cos(\mu_b)-j\sigma_b^2[\tan(\mu_b)]^{-1}T_b\Delta\omega]\times \exp\left[-j[\sin(\mu_b)]^{-1}T_b\Delta\omega - 0.5\sigma_b^2[\sin(\mu_b)\tan(\mu_b)]^{-2}T_b^2(\Delta\omega)^2\right] + (1-\Lambda_b)[\cos(\mu_s)+j\sigma_s^2[\tan(\mu_s)]^{-1}T_s\Delta\omega]\times \exp\left[j[\sin(\mu_s)]^{-1}T_s\Delta\omega - 0.5\sigma_s^2[\sin(\mu_s)\tan(\mu_s)]^{-2}T_s^2(\Delta\omega)^2\right]. \quad (49)$$

For $\Delta f = 0$, (48) and (49) simplify to the results given in a previous subsection. The magnitudes of (48) and (49) are plotted in Fig. 6.

(c) Velocity Correlations: When (31)-(33) are applied to (37), we obtain the following results at $L=0$, respectively

$$E[P_1^z(f+\Delta f)\{P_1^z(f)\}^*] = \Lambda_b\begin{bmatrix}\sin^2(\mu_b)+\sigma_b^2\cos^2(\mu_b)-\sigma_b^4[\tan(\mu_b)]^{-4}T_b^2(\Delta\omega)^2\\ +j2\sigma_b^2\cos^2(\mu_b)[\sin(\mu_b)]^{-1}T_b\Delta\omega\end{bmatrix} \exp\left[-j[\sin(\mu_b)]^{-1}T_b\Delta\omega - 0.5\sigma_b^2[\sin(\mu_b)\tan(\mu_b)]^{-2}T_b^2(\Delta\omega)^2\right] + (1-\Lambda_b)\begin{bmatrix}\sin^2(\mu_s)+\sigma_s^2\cos^2(\mu_s)-\sigma_s^4[\tan(\mu_s)]^{-4}T_s^2(\Delta\omega)^2\\ -j2\sigma_s^2\cos^2(\mu_s)[\sin(\mu_s)]^{-1}T_s\Delta\omega\end{bmatrix} \exp\left[j[\sin(\mu_s)]^{-1}T_s\Delta\omega - 0.5\sigma_s^2[\sin(\mu_s)\tan(\mu_s)]^{-2}T_s^2(\Delta\omega)^2\right], \quad (50)$$

$$E[P_1^y(f+\Delta f)\{P_1^y(f)\}^*] = \Lambda_b\begin{bmatrix}\cos^2(\mu_b)+\sigma_b^2\sin^2(\mu_b)-\sigma_b^4[\tan(\mu_b)]^{-2}T_b^2(\Delta\omega)^2\\ -j2\sigma_b^2\cos^2(\mu_b)[\sin(\mu_b)]^{-1}T_b\Delta\omega\end{bmatrix} \exp\left[-j[\sin(\mu_b)]^{-1}T_b\Delta\omega - 0.5\sigma_b^2[\sin(\mu_b)\tan(\mu_b)]^{-2}T_b^2(\Delta\omega)^2\right] + (1-\Lambda_b)\begin{bmatrix}\cos^2(\mu_s)+\sigma_s^2\sin^2(\mu_s)-\sigma_s^4[\tan(\mu_s)]^{-2}T_s^2(\Delta\omega)^2\\ +j2\sigma_s^2\cos^2(\mu_s)[\sin(\mu_s)]^{-1}T_s\Delta\omega\end{bmatrix} \exp\left[j[\sin(\mu_s)]^{-1}T_s\Delta\omega - 0.5\sigma_s^2[\sin(\mu_s)\tan(\mu_s)]^{-2}T_s^2(\Delta\omega)^2\right], \quad (51)$$

$$E[P_1^z(f+\Delta f)\{P_1^y(f)\}^*] = \Lambda_b\begin{bmatrix}(1-\sigma_b^2)\sin(\mu_b)\cos(\mu_b)+\sigma_b^4[\tan(\mu_b)]^{-3}T_b^2(\Delta\omega)^2\\ -j\sigma_b^2[\cos(\mu_b)-\cos^3(\mu_b)[\sin(\mu_b)]^{-1}]T_b\Delta\omega\end{bmatrix} \exp\left[-j[\sin(\mu_b)]^{-1}T_b\Delta\omega - 0.5\sigma_b^2[\sin(\mu_b)\tan(\mu_b)]^{-2}T_b^2(\Delta\omega)^2\right] + (1-\Lambda_b)\begin{bmatrix}(1-\sigma_s^2)\sin(\mu_s)\cos(\mu_s)+\sigma_s^4[\tan(\mu_s)]^{-3}T_s^2(\Delta\omega)^2\\ +j\sigma_s^2[\cos(\mu_s)-\cos^3(\mu_s)[\sin(\mu_s)]^{-1}]T_s\Delta\omega\end{bmatrix} \exp\left[j[\sin(\mu_s)]^{-1}T_s\Delta\omega - 0.5\sigma_s^2[\sin(\mu_s)\tan(\mu_s)]^{-2}T_s^2(\Delta\omega)^2\right]. \quad (52)$$

When $\Delta f = 0$, (50)-(52) reduce to (44)-(46). The plots of the magnitudes of (50)-(52) are given in Fig. 7.

In the ambient noise field, correlations among the elements of a vector sensor array are calculated in [23]. The emphasis of this paper, however, is the development of a geometrical-statistical model for the shallow water waveguide, as shown in Fig. 2 and analyzed in appendices. Upon using Gaussian PDFs for surface- and bottom-reflected AOAs, a closed-form integral-free expression is derived in (37) for the pressure field correlation in space and frequency. Another focal point of the present paper is the emphasis on the frequency domain representation of the acoustic field, e.g., the frequency transfer functions in (8) and (9). This allows to derive frequency

domain correlations that are important for communication system design. For example, eq. (47) can be used to determine the correlation between two Δf -separated tones received by a vector sensor, in a multi-carrier system such as OFDM (orthogonal frequency division multiplexing). Overall, the proposed shallow water geometrical-statistical channel model provides useful expressions for space-frequency vector sensor correlations, in terms of the physical parameters of the channel such as mean angle of arrivals and angle spreads.

VI. Comparison with Experimental Data

To experimentally verify the proposed model, in this section we compare the derived pressure correlation function in (38) with the measured data of [24]. Once the accuracy of the pressure correlation function is experimentally confirmed, one can take the derivatives of the pressure correlation, to find different types of correlations in a vector sensor array, as discussed in previous sections.

A uniform 33-element array with 0.5 m element spacing was deployed at a 10 km range, where the bottom depth was 103 m [24]. The measurements were conducted at the center frequency of $f_0 = 1.2$ kHz . The empirical vertical correlation of the pressure field, estimated from the measured data, is shown in Fig. 8. The vertical correlation in [24] is measured with respect to the eighth element from the bottom of the 33-element array. This explains the horizontal axis in Fig. 8 and the peak value at the eight element. To compare the proposed correlation model in (38) with measured correlation, its parameters need to be determined. We chose $\mu_b = 3^o$ and $\mu_s = 353^o \equiv -7^o$, as according to [24], there are two dominant arrivals from these directions. After inserting these numbers into (38), the remaining parameters were estimated using a numerical least squares approach. Similarly to [24], the model was compared with the measured correlation over the eight neighboring receivers (elements one to fifteen in Fig. 8). This resulted in $\Lambda_b = 0.56$, $\sigma_b = 0.04$ and $\sigma_s = 0.14$ rad . The magnitude of the proposed model in (38) is plotted in Fig. 8. The close agreement between the model and measured correlations in Fig. 8 indicates the usefulness of the model. As a reference, the exponential model of [24], i.e., $\exp(-L^2/(2\lambda)^2)$ is also included in Fig. 8. Here $\lambda = 1.2$ m is the wavelength. One can observe the proposed model provides a closer match to experimental correlation at the first and fifteenth elements. The main advantage of the proposed model is that it expresses the acoustic field correlation as a function of important physical parameters of the channel such as angle of arrivals and angle spreads. This allows system engineers to understand how these channel parameters affect the correlation, which in turn provides useful guidelines for array and system design.

VII. Discussion

Overall, depending on the AOA of the pressure wave, correlations among pressure and velocity components vary. In the numerical example of Section V, the mean AOA of impinging waves is almost horizontal, as shown in Fig. 3. This is why in Fig. 4 and Fig. 6, crosscorrelation among P and P^y channels are high, whereas P and P^z channels are less correlated. Fig. 5 and Fig. 7 further confirm that P^y and P^z channels are almost uncorrelated.

To further confirm the above argument, let us focus on a single vector sensor. Without loss of generality we consider $\Lambda_b = 1$. Then according to the paragraph immediately after (40), P/P^y and P/P^z crosscorrelations are given by $\cos(\mu_b)$ and $\sin(\mu_b)$, respectively. For small values of μ_b , i.e., mostly horizontal wave propagation towards the receiver, we note that P/P^y crosscorrelation is high whereas P/P^z crosscorrelation is small. On the other hand, as μ_b approaches 90^o , i.e., nearly vertical AOAs, P/P^y crosscorrelation becomes small whereas P/P^z crosscorrelation is large.

To look at the P^y/P^z crosscorrelattion under the above setup, we use (46), which results in a crosscorrelation proportional to $\sin(2\mu_b)$. As expected, for the two extreme cases of mostly horizontal ($\mu_b \approx 0^o$) and vertical ($\mu_b \approx 90^o$) AOAs, P^y and P^z are almost uncorrelated. Crosscorrelation between P^y and P^z reaches its maximum when $\mu_b = 45^o$, as expected. This is the case where AOAs are not biased towards horizontal and vertical directions.

Vector sensor correlations that are calculated in this paper provide useful guidelines which are highly needed for transceiver design. For example, in the numerical example of Section V, also discussed at the beginning of this section, the y and z components of the acoustic particle velocity are nearly uncorrelated for different element spacings L and frequency separations Δf . This is true even for $L = 0$, i.e., a single vector sensor. This means that y and z channels of a single vector sensor receiver can provide a diversity gain of order two in our numerical example, which in turn reduces the symbol detection error probability.

It is noteworthy that a vector sensor measures the vector components of the acoustic field such as the velocity channels, all at a single point in space. Therefore, the above new type of diversity is provided by two co-located particle velocity channels, measured by a single vector sensor receiver. To achieve diversity, traditionally arrays of spatially separated pressure sensors are used in underwater acoustic communication. The large size of the pressure sensor arrays in some situations, however, may prohibit them from being used in applications where the receiver size is a serious limitation. Examples include small unmanned underwater vehicles for offshore oil exploration, oceanographic studies, environmental monitorings, etc. The diversity offered by vector sensors make them particularly suitable for such applications.

VIII. Conclusion

In this paper we have developed a statistical/geometrical framework for mathematical characterization of acoustic vector sensor array correlations in shallow waters. Closed-form expressions are derived which relate signal correlations to some key channel parameters such as mean angle of arrivals

and angle spreads. Using these expressions one can calculate the correlations between the pressure and velocity channels of the sensors, in terms of element spacing and frequency separation. The results of this paper are useful for the design and performance analysis of vector sensor communication systems and array processing algorithms. The interested reader can refer to [8] and [9] for the principles and concepts of communication with vector sensors and particle velocity channels. Moreover, a vector sensor multiuser system that does not use spreading codes and bandwidth expansion is developed in [10]. This system can be particularly useful for highly bandlimited underwater channels.

ACKNOWLEDGEMENT

We thank Dr. T. C. Yang from the Naval Research Laboratory, Washington, DC, for useful discussions regarding experimental data and the underwater spatial correlation.

Appendix I.

A CLOSED-FORM FREQUENCY-SPACE CORRELATION MODEL FOR THE PRESSURE CHANNEL

When angle spreads are small and $L \ll \min(z_1, D_0 - z_1)$, one can approximate the AOAs in (8) and (9) as $\gamma_{i,1}^b \approx \gamma_{i,2}^b \approx \gamma_i^b$ and $\gamma_{m,1}^s \approx \gamma_{m,2}^s \approx \gamma_m^s$, where γ_i^b and γ_m^s are shown in Fig. 2. Furthermore, the traveled distances can be approximated as $\xi_{i,1}^b \approx \xi_{i,2}^b \approx \xi_i^b$ and $\xi_{m,1}^s \approx \xi_{m,2}^s \approx \xi_m^s$, with ξ_i^b and ξ_m^s depicted in Fig. 2 (higher order approximations are provided in Appendix III). Note that each delay is the traveled distance divided by the sound speed *c*. Therefore all the delays in (8) and (9) can be approximated by $\tau_{i,1}^b \approx \tau_{i,2}^b \approx \tau_i^b$ and $\tau_{m,1}^s \approx \tau_{m,2}^s \approx \tau_m^s$, where $\tau_i^b = \xi_i^b / c$ and $\tau_m^s = \xi_m^s / c$. According to Fig. 2 it is easy to verify that $\sin(\gamma_i^b) = (D_0 - D)/\xi_i^b$ and $-\sin(\gamma_m^s) = D/\xi_m^s$. Hence

$$\tau_i^b = T_b / \sin(\gamma_i^b),\ 0 < \gamma_i^b < \pi,\quad \tau_m^s = -T_s / \sin(\gamma_m^s),\ \pi < \gamma_m^s < 2\pi. \tag{53}$$

The parameters $T_b = (D_0 - D)/c$ and $T_s = D/c$ in (53) denote the vertical travel times from the sea bottom to the array center, and from the sea surface to the array center, respectively. Clearly the range of γ_m^s in (53) implies that $-1 \le \sin(\gamma_m^s) < 0$, which makes τ_m^s non-negative, as expected. In general we have $T_b \le \tau_i^b < \infty$, $\forall i$, and $T_s \le \tau_m^s < \infty$, $\forall m$. Now (8) and (9) can be simplified to the equations given in (54) and (55), where $\varepsilon_y > 0$ is a displacement in the *y* direction. Note that ε_y is introduced to represent the location of the second sensor in Fig. 2 as $(y, z) = (\varepsilon_y, z_1 + L)$, as $\varepsilon_y \to 0$. This allows to calculate those correlation functions which are related to the horizontal component of the velocity, as discussed in Section IV.

$$\begin{aligned} P_1(f) &= (\Lambda_b / N^b)^{1/2} \\ &\times \sum_{i=1}^{N^b} a_i^b \exp(j\psi_i^b) \exp(jk\, z_1 \sin(\gamma_i^b)) \exp(-jT_b\omega / \sin(\gamma_i^b)) \\ &\quad + ((1-\Lambda_b)/N^s)^{1/2} \\ &\times \sum_{m=1}^{N^s} a_m^s \exp(j\psi_m^s) \exp(jk\, z_1 \sin(\gamma_m^s)) \exp(jT_s\omega / \sin(\gamma_m^s)), \end{aligned} \tag{54}$$

$$\begin{aligned} P_2(f) &= (\Lambda_b / N^b)^{1/2} \sum_{i=1}^{N^b} a_i^b \exp(j\psi_i^b) \\ &\exp(jk[\varepsilon_y \cos(\gamma_i^b) + (z_1 + L)\sin(\gamma_i^b)]) \exp(-jT_b\omega / \sin(\gamma_i^b)) \\ &\quad + ((1-\Lambda_b)/N^s)^{1/2} \sum_{m=1}^{N^s} a_m^s \exp(j\psi_m^s) \\ &\exp(jk[\varepsilon_y \cos(\gamma_m^s) + (z_1 + L)\sin(\gamma_m^s)]) \exp(jT_s\omega / \sin(\gamma_m^s)), \\ &\qquad \text{as } \varepsilon_y \to 0. \end{aligned} \tag{55}$$

Due to the uniform distribution of all the phases $\{\psi_i^b\}_i$ and $\{\psi_m^s\}_m$ over $[0, 2\pi)$ we have $E[\exp(\pm j\psi_i^b)] = E[\exp(\pm j\psi_m^s)] = 0,\ \forall i, m$. This results in $E[\exp(\pm j\psi_i^b)\exp(\pm j\psi_m^s)] = 0,\ \forall i, m$, because all the phases are independent. Similarly we have $E[\exp(j\psi_i^b)\exp(-j\psi_{\tilde{i}}^b)] = 0,\ \forall i \ne \tilde{i}$ and $E[\exp(j\psi_m^s)\exp(-j\psi_{\tilde{m}}^s)] = 0,\ \forall m \ne \tilde{m}$. Clearly the last two expressions become 1, when $i = \tilde{i}$ and $m = \tilde{m}$. Therefore, after substituting (54) and (55) into $C_P(\Delta f, L) = E[P_2(f + \Delta f) P_1^*(f)]$, only the following two single summations remain

$$\begin{aligned} C_P(\Delta f, L) &= (\Lambda_b / N^b) \sum_{i=1}^{N^b} E[(a_i^b)^2] \\ &\times \exp(jk[\varepsilon_y \cos(\gamma_i^b) + L\sin(\gamma_i^b)]) \exp(-jT_b \Delta\omega / \sin(\gamma_i^b)) \\ &\quad + ((1-\Lambda_b)/N^s) \sum_{m=1}^{N^s} E[(a_m^s)^2] \\ &\times \exp(jk[\varepsilon_y \cos(\gamma_m^s) + L\sin(\gamma_m^s)]) \exp(jT_s \Delta\omega / \sin(\gamma_m^s)), \\ &\qquad \text{as } \varepsilon_y \to 0, \end{aligned} \tag{56}$$

where $\Delta\omega = 2\pi\,\Delta f$.

The terms $E[(a_i^b)^2]/N^b$ and $E[(a_m^s)^2]/N^s$ in (56) represent the normalized (average) powers received from the two scatterers S_i^b and S_m^s on the sea bottom and its surface, respectively. Let $\sum_{i=1}^{N^b} E[(a_i^b)^2]/N^b = 1$ and $\sum_{m=1}^{N^s} E[(a_m^s)^2]/N^s = 1$. We also define $w_{\text{bottom}}(\gamma^b)$ and $w_{\text{surface}}(\gamma^s)$ as the probability density functions (PDFs) of the AOAs of the waves coming from the sea bottom and its surface, respectively, such that $0 < \gamma^b < \pi$ and $\pi < \gamma^s < 2\pi$. When N^b and N^s are large, one can think of $E[(a_i^b)^2]/N^b$ and $E[(a_m^s)^2]/N^s$ as the normalized powers received through the infinitesimal angles $d\gamma^b$ and $d\gamma^s$, respectively, centered at the AOAs γ_i^b and γ_m^s. Thus, with the chosen normalizations $\sum_{i=1}^{N^b} E[(a_i^b)^2]/N^b = 1$ and $\sum_{m=1}^{N^s} E[(a_m^s)^2]/N^s = 1$, we can write $E[(a_i^b)^2]/N^b = w_{\text{bottom}}(\gamma_i^b) d\gamma^b$ and $E[(a_m^s)^2]/N^s = w_{\text{surface}}(\gamma_m^s) d\gamma^s$. These relations allow the summations in (56) to be replaced by integrals

$$\begin{aligned} C_P(\Delta f, L) &= \Lambda_b \int_{\gamma^b=0}^{\pi} w_{\text{bottom}}(\gamma^b) \exp(-jT_b\Delta\omega / \sin(\gamma^b)) \\ &\quad \times \exp(jk[\varepsilon_y \cos(\gamma^b) + L\sin(\gamma^b)]) d\gamma^b \\ &\quad + (1-\Lambda_b) \int_{\gamma^s=\pi}^{2\pi} w_{\text{surface}}(\gamma^s) \exp(jT_s\Delta\omega / \sin(\gamma^s)) \\ &\quad \times \exp(jk[\varepsilon_y \cos(\gamma^s) + L\sin(\gamma^s)]) d\gamma^s,\ \text{as } \varepsilon_y \to 0. \end{aligned} \tag{57}$$

Note that according to (57) we have $C_P(0,0) = \Lambda_b + (1-\Lambda_b) = 1$, which represents the convenient unit (total average) received pressure power. The factor

$0 \le \Lambda_b \le 1$ was defined to stand for the amount of the power coming from the sea bottom, whereas $1-\Lambda_b$ shows the power coming from the surface.

Appendix II.

The Exact Frequency-Space Correlation of the Pressure Channel

Here we derive the exact frequency-space correlation of the pressure channel, for the vertical array in the shallow water channel of Fig. 2. By inserting $P_1(f)$ and $P_2(f)$ from (8) and (9) into $C_P(\Delta f, L) = E[P_2(f+\Delta f)P_1^*(f)]$ and upon using the properties of the phases $\{\psi_i^b\}_i$ and $\{\psi_m^s\}_m$, as done in Appendix I, one can show that

$$\begin{aligned} C_P(\Delta f, L) &= (\Lambda_b / N^b)\sum_{i=1}^{N^b} E[(a_i^b)^2] \\ &\times \exp(jkz_1[\sin(\gamma_{i,2}^b) - \sin(\gamma_{i,1}^b)])\exp(jkL\sin(\gamma_{i,2}^b)) \\ &\times \exp(-j\Delta\omega\tau_{i,2}^b)\exp(j\omega(\tau_{i,1}^b - \tau_{i,2}^b)) \\ &+ ((1-\Lambda_b)/N^s)\sum_{m=1}^{N^s} E[(a_m^s)^2] \\ &\times \exp(jkz_1[\sin(\gamma_{m,2}^s) - \sin(\gamma_{m,1}^s)])\exp(jkL\sin(\gamma_{m,2}^s)) \\ &\times \exp(-j\Delta\omega\tau_{m,2}^s)\exp(j\omega(\tau_{m,1}^s - \tau_{m,2}^s)). \end{aligned} \tag{58}$$

By using the law of cosines in appropriate triangles in Fig. 2, one can obtain the following relations, which are needed for calculating (58), numerically

$$\sin(\gamma_{i,1}^b) = \frac{(D_0 - z_1)\sin(\gamma_i^b)}{\sqrt{(D_0 - z_1 - 0.5L)^2 + L(D_0 - z_1 - 0.25L)\sin^2(\gamma_i^b)}} \tag{59}$$

$$\sin(\gamma_{i,2}^b) = \frac{(D_0 - z_1 - L)\sin(\gamma_i^b)}{\sqrt{(D_0 - z_1 - 0.5L)^2 - L(D_0 - z_1 - 0.75L)\sin^2(\gamma_i^b)}} \tag{60}$$

$$\tau_{i,1}^b = \frac{\xi_{i,1}^b}{c} = \frac{\sqrt{(D_0 - z_1 - 0.5L)^2 + L(D_0 - z_1 - 0.25L)\sin^2(\gamma_i^b)}}{c\sin(\gamma_i^b)} \tag{61}$$

$$\tau_{i,2}^b = \frac{\xi_{i,2}^b}{c} = \frac{\sqrt{(D_0 - z_1 - 0.5L)^2 - L(D_0 - z_1 - 0.75L)\sin^2(\gamma_i^b)}}{c\sin(\gamma_i^b)} \tag{62}$$

$$\sin(\gamma_{m,1}^s) = \frac{z_1\sin(\gamma_m^s)}{\sqrt{(z_1 + (L/2))^2 - L(z_1 + (L/4))\sin^2(\gamma_m^s)}}, \tag{63}$$

$$\sin(\gamma_{m,2}^s) = \frac{(z_1 + L)\sin(\gamma_m^s)}{\sqrt{(z_1 + (L/2))^2 + L(z_1 + (3L/4))\sin^2(\gamma_m^s)}}, \tag{64}$$

$$\tau_{m,1}^s = \frac{\xi_{m,1}^s}{c} = \frac{-\sqrt{(z_1 + (L/2))^2 - L(z_1 + (L/4))\sin^2(\gamma_m^s)}}{c\sin(\gamma_m^s)}, \tag{65}$$

$$\tau_{m,2}^s = \frac{\xi_{m,2}^s}{c} = \frac{-\sqrt{(z_1 + (L/2))^2 + L(z_1 + (3L/4))\sin^2(\gamma_m^s)}}{c\sin(\gamma_m^s)}. \tag{66}$$

All the sin's and τ's in (59)-(66) are functions of the bottom and surface AOAs γ_i^b and γ_m^s, respectively. As done in Appendix I, when N^b and N^s are large, one can introduce the AOA PDFs as $E[(a_i^b)^2]/N^b = w_{\text{bottom}}(\gamma_i^b)d\gamma^b$ and $E[(a_m^s)^2]/N^s = w_{\text{surface}}(\gamma_m^s)d\gamma^s$. This way the two summations in (58) can be replaced by integrals over γ^b and γ^s, respectively

$$\begin{aligned} C_P(\Delta f, L) &= \Lambda_b\int_{\gamma^b=0}^{\pi} w_{\text{bottom}}(\gamma^b)\exp(jkz_1[\sin(\gamma_2^b) - \sin(\gamma_1^b)]) \\ &\times \exp(jkL\sin(\gamma_2^b))\exp(-j\Delta\omega\tau_2^b)\exp(j\omega(\tau_1^b - \tau_2^b))\,d\gamma^b \\ &+ (1-\Lambda_b)\int_{\gamma^s=\pi}^{2\pi} w_{\text{surface}}(\gamma^s)\exp(jkz_1[\sin(\gamma_2^s) - \sin(\gamma_1^s)]) \\ &\times \exp(jkL\sin(\gamma_2^s))\exp(-j\Delta\omega\tau_2^s)\exp(j\omega(\tau_1^s - \tau_2^s))\,d\gamma^s. \end{aligned} \tag{67}$$

Note that all the sin's and τ's in (67) are exactly the same as those given in (59)-(66), with the subscripts *i* and *m* removed.

Appendix III.

Higher Order Approximations

In Appendix I the AOAs and traveled distances of Fig. 2 are approximated as $\gamma_{i,1}^b \approx \gamma_{i,2}^b \approx \gamma_i^b$, $\gamma_{m,1}^s \approx \gamma_{m,2}^s \approx \gamma_m^s$, $\xi_{i,1}^b \approx \xi_{i,2}^b \approx \xi_i^b$ and $\xi_{m,1}^s \approx \xi_{m,2}^s \approx \xi_m^s$. This resulted in the frequency-space pressure field correlation model in (12), whose integrals can be analytically solved for Gaussian AOAs. The resulting formula is given in (37). By using the higher order approximations of this appendix, a closed-form and integral-free correlation formula which is closer to the exact expression in (67) can be obtained for a vertical array.

When $L \ll \min(z_1, D_0 - z_1)$, sin of AOAs of Fig. 2, given in (59), (60), (63) and (64) can be approximated by

$$\begin{aligned} \sin(\gamma_{i,1}^b) &\approx \sin(\gamma_i^b)[1 - 0.5L\sin^2(\gamma_i^b)/(D_0 - z_1)], \\ \sin(\gamma_{i,2}^b) &\approx \sin(\gamma_i^b)[1 + 0.5L\sin^2(\gamma_i^b)/(D_0 - z_1)], \\ \sin(\gamma_{m,1}^s) &\approx \sin(\gamma_m^s)[1 + 0.5L\sin^2(\gamma_m^s)/z_1], \\ \sin(\gamma_{m,2}^s) &\approx \sin(\gamma_m^s)[1 - 0.5L\sin^2(\gamma_m^s)/z_1]. \end{aligned} \tag{68}$$

Equation (68) is obtained according to $1/\sqrt{1+x} \approx 1-(x/2)$ when $|x| \ll 1$. Similarly, using $\sqrt{1+x} \approx 1+(x/2)$ for $|x| \ll 1$, the traveled distances ξ's of Fig. 2, listed in (61), (62), (65) and (66) can be approximated as

$$\begin{aligned} \xi_{i,1}^b &\approx [(D_0 - z_1) + 0.5L\sin^2(\gamma_i^b)]/\sin(\gamma_i^b), \\ \xi_{i,2}^b &\approx [(D_0 - z_1) - 0.5L\sin^2(\gamma_i^b)]/\sin(\gamma_i^b), \\ \xi_{m,1}^s &\approx -[z_1 - 0.5L\sin^2(\gamma_m^s)]/\sin(\gamma_m^s), \\ \xi_{m,2}^s &\approx -[z_1 + 0.5L\sin^2(\gamma_m^s)]/\sin(\gamma_m^s). \end{aligned} \tag{69}$$

Based on (68) and (69) it is easy to verify

$$\begin{aligned} \sin(\gamma_{i,2}^b) - \sin(\gamma_{i,1}^b) &\approx L\sin^3(\gamma_i^b)/(D_0 - z_1), \\ \sin(\gamma_{m,2}^s) - \sin(\gamma_{m,1}^s) &\approx -L\sin^3(\gamma_m^s)/z_1, \\ \tau_{i,1}^b - \tau_{i,2}^b &\approx L\sin(\gamma_i^b)/c, \\ \tau_{m,1}^s - \tau_{m,2}^s &\approx L\sin(\gamma_m^s)/c. \end{aligned} \tag{70}$$

By substituting (68)-(70) in (58) and changing the summations to integrals, a new frequency-space correlation similar to (12) can be obtained for a vertical array, which of course has more terms. By considering small angle spreads, a Taylor expansion similar to (35) for $\sin^3(.)$ and finally Gaussian AOA distributions, the bottom and surface integrals in the new frequency-space correlation can be analytically

solved (recall the characteristic function of a zero-mean Gaussian variable used to derive (37), i.e., $\int \exp(j\theta x)(2\pi\sigma^2)^{-1/2}\exp[-x^2/(2\sigma^2)]dx = \exp(-\sigma^2\theta^2/2)$ [20]). The new closed-from frequency-space pressure correlation, not provided here due to space limitations, is a more accurate yet more complex integral-free alternative to (37).

REFERENCES

[1] A. Nehorai and E. Paldi, "Acoustic vector-sensor array processing," *IEEE Trans. Signal Processing*, vol. 42, pp. 2481-2491, 1994.

[2] B. Hochwald and A. Nehorai, "Identifiably in array processing models with vector-sensor applications," *IEEE Trans. Signal Processing*, vol. 44, pp. 83-95, 1996.

[3] K. T. Wong and M. D. Zoltowski, "Self-Initiating MUSIC-based direction finding in underwater acoustic particle velocity-field beamspace," *IEEE J. Oceanic Eng.*, vol. 25, pp. 262-273, 2000.

[4] B. A. Cray and A. H. Nuttall, "Directivity factors for linear arrays of velocity sensors," *J. Acoust. Soc. Am.*, vol. 110, pp. 324-331, 2001.

[5] M. Hawkes and A. Nehorai, "Wideband source localization using a distributed acoustic vector-sensor array," *IEEE Trans. Signal Processing*, vol. 51, pp. 1479-1491, 2003.

[6] *Proc. AIP Conf. Acoustic Particle Velocity Sensors: Design, Performance, and Applications*, Mystic, CT, 1995.

[7] *Proc. Workshop Directional Acoustic Sensors (CD-ROM)*, New Port, RI, 2001.

[8] A. Abdi and H. Guo, "A new compact multichannel receiver for underwater wireless communication networks," accepted for publication in *IEEE Trans. Wireless Commun.*, 2008.

[9] A. Abdi, H. Guo and P. Sutthiwan, "A new vector sensor receiver for underwater acoustic communication," in *Proc. MTS/IEEE Oceans*, Vancouver, BC, Canada, 2007.

[10] H. Guo and A. Abdi, "Multiuser underwater communication with space-time block codes and acoustic vector sensors," in *Proc. MTS/IEEE Oceans*, Quebec City, QC, Canada, 2008.

[11] M. O. Damen, A. Abdi, and M. Kaveh, "On the effect of correlated fading on several space-time coding and detection schemes," in *Proc. IEEE Vehic. Technol. Conf.*, Atlantic City, NJ, 2001, pp. 13-16.

[12] M. Chiani, M. Z. Win and A. Zanella, "On the capacity of spatially correlated MIMO Rayleigh-fading channels," *IEEE Trans. Inform. Theory*, vol. 49, pp. 2363-2371, 2003.

[13] V. K. Nguyen and L. B. White, "Joint space-time trellis decoding and channel estimation in correlated fading channels," *IEEE Signal Processing Lett.*, vol. 11, pp. 633-636, 2004.

[14] A. Abdi and M. Kaveh, "Parametric modeling and estimation of the spatial characteristics of a source with local scattering," in *Proc. IEEE Int. Conf. Acoust., Speech, Signal Processing*, Orlando, FL, 2002, pp. 2821-2824.

[15] C. B. Ribeiro, E. Ollila and V. Koivunen, "Stochastic maximum-likelihood method for MIMO propagation parameter estimation," *IEEE Trans. Signal Processing*, vol. 55, pp. 46-55, 2007.

[16] B. A. Cray, V. M. Evora, and A. H. Nuttall, "Highly directional acoustic receivers," *J. Acoust. Soc. Am.*, vol. 113, pp. 1526-1532, 2003.

[17] A. D. Pierce, *Acoustics: An Introduction to Its Physical Principles and Applications*, 2nd ed., Acoustic Soc. Am., 1989.

[18] P. C. Etter, *Underwater Acoustic Modeling and Simulation*, 3rd ed., New York: Spon, 2003.

[19] H. L. Van Trees, *Optimum Array Processing*. New York: Wiley, 2002.

[20] A. Papoulis, *Probability, Random Variables, and Stochastic Processes*, 3rd ed., Singapore: McGraw-Hill, 1991.

[21] A. Abdi, J. A. Barger, and M. Kaveh, "A parametric model for the distribution of the angle of arrival and the associated correlation function and power spectrum at the mobile station," *IEEE Trans. Vehic. Technol.*, vol. 51, pp. 425-434, 2002.

[22] A. Abdi and M. Kaveh, "A space-time correlation model for multielement antenna systems in mobile fading channels," *IEEE J. Select. Areas Commun.*, vol. 20, pp. 550-560, 2002.

[23] M. Hawkes and A. Nehorai, "Acoustic vector-sensor correlations in ambient noise," *IEEE J. Oceanic Eng.*, vol. 26, pp. 337-347, 2001.

[24] T. C. Yang, "A study of spatial processing gain in underwater acoustic communications," *IEEE J. Oceanic Eng.*, vol. 32, pp. 689-709, 2007.

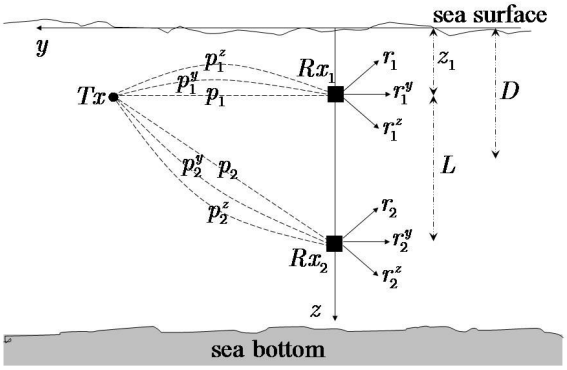

Fig. 1. A vector sensor system with one pressure transmitter and two vector sensor receivers. Each vector sensor measures the pressure, as well as the y and z component of the acoustic particle velocity, all in a single point.

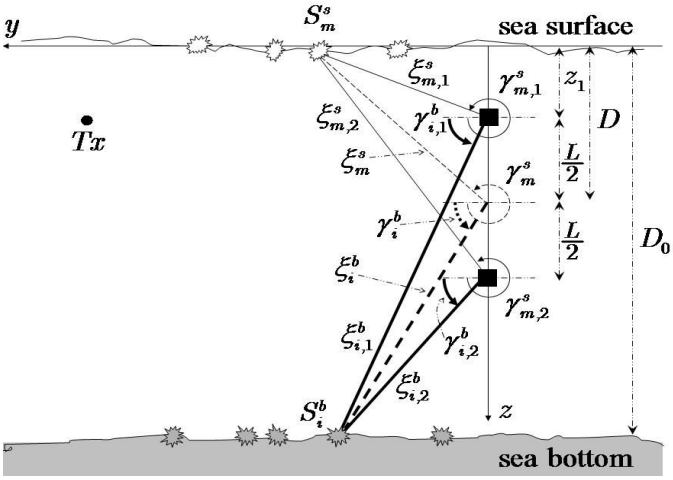

Fig. 2. Geometrical representation of the received rays at the two vector sensors in a shallow water multipath channel.

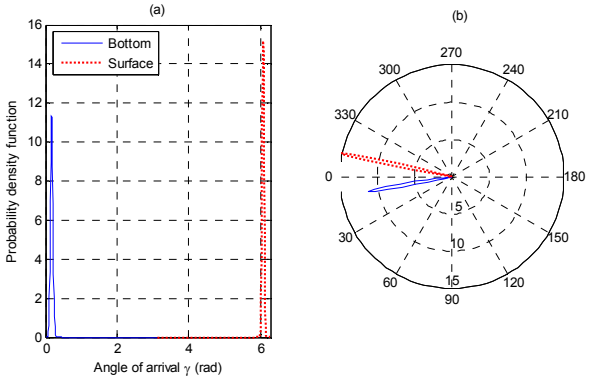

Fig. 3. The bottom and surface angle-of-arrival Gaussian PDFs in (34), with $\sigma_b = \pi/90$ (2°), $\mu_b = \pi/18$ (10°), $\sigma_s = \pi/120$ (1.5°) and $\mu_s = 348\pi/180$ (348° ≡ −12°) : (a) linear plot, (b) polar plot.

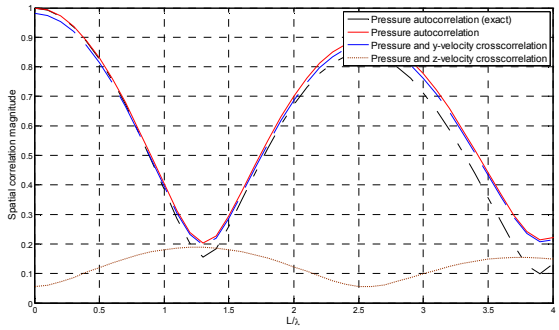

Fig. 4. The magnitudes of the pressure spatial autocorrelation in (38) and pressure-velocity spatial crosscorrelations in (39) and (40) versus L/λ, with $\Lambda_b = 0.4$, $\sigma_b = \pi/90$ (2°), $\mu_b = \pi/18$ (10°), $\sigma_s = \pi/120$ (1.5°), $\mu_s = 348\pi/180$ (348° ≡ −12°).

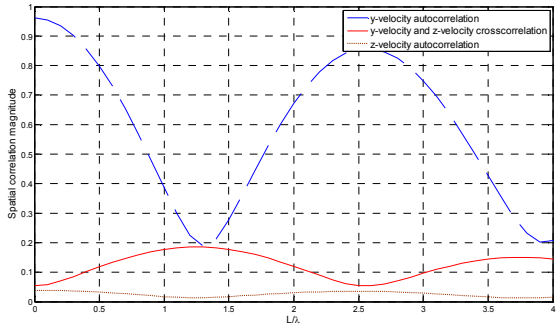

Fig. 5. The magnitudes of the velocity spatial autocorrelations in (41) and (42), and velocity-velocity spatial crosscorrelation in (43) versus L/λ, with $\Lambda_b = 0.4$, $\sigma_b = \pi/90$ (2°), $\mu_b = \pi/18$ (10°), $\sigma_s = \pi/120$ (1.5°), $\mu_s = 348\pi/180$ (348° ≡ −12°).

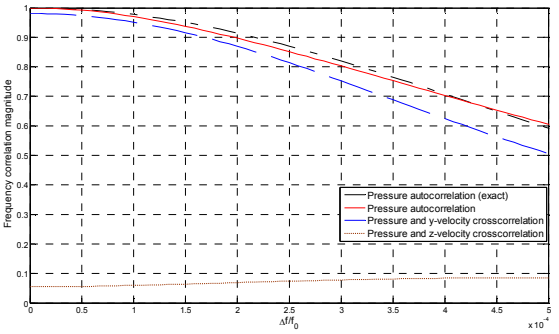

Fig. 6. The magnitudes of the pressure frequency autocorrelation in (47) and the pressure-velocity frequency crosscorrelations in (48) and (49) versus $\Delta f/f_0$, with $f_0 = 12$ kHz, $D_0 = 100$ m, $z_1 = 54$ m, $c = 1500$ m/s, $\Lambda_b = 0.4$, $\sigma_b = \pi/90$ (2°), $\mu_b = \pi/18$ (10°), $\sigma_s = \pi/120$ (1.5°), $\mu_s = 348\pi/180$ (348° ≡ −12°).

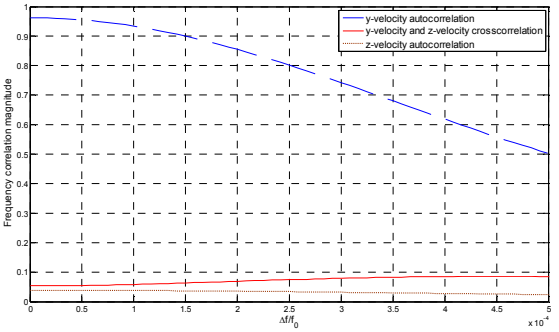

Fig. 7. The magnitudes of the velocity frequency autocorrelations in (50) and (51), and velocity-velocity frequency crosscorrelation in (52) versus $\Delta f/f_0$, with $f_0 = 12$ kHz, $D_0 = 100$ m, $z_1 = 54$ m, $c = 1500$ m/s, $\Lambda_b = 0.4$, $\sigma_b = \pi/90$ (2°), $\mu_b = \pi/18$ (10°), $\sigma_s = \pi/120$ (1.5°), $\mu_s = 348\pi/180$ (348° ≡ −12°).

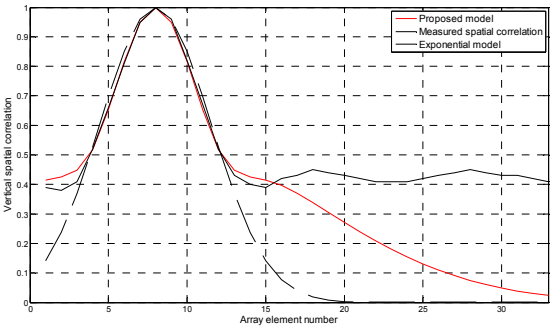

Fig. 8. Comparison of the proposed model with measured data.